Ab initio lattice dynamics of $MgSiO_3$ perovskite at high pressure

B. B. Karki and R. M. Wentzcovitch
Department of Chemical Engineering and Materials Science, Minnesota Supercomputing Institute, University of Minnesota, Minneapolis, Minnesota 55455

S. de Gironcoli and S. Baroni
Scuola Internazionale Superiore di Studi Avanzati (SISSA), Instituto Nazionale Fisica della Materia (INFM), I-34014 Trieste, Italy
(Received 19 July 2000)

Phonon dispersions of $MgSiO_3$ perovskite are calculated as a function of pressure up to 150 GPa using density-functional perturbation theory. Predicted zone-center frequencies and their pressure shifts are in close correspondence with existing Raman and infrared data, even though identification of the measured modes may be ambiguous. It is shown that the frequencies increase monotonically with pressure and no soft modes exist over the pressure regime studied. Low-frequency modes appear to be primarily associated with the SiO_6 octahedral libration and large Mg displacement whereas high-frequency modes are dominated by octahedral deformation. The calculated frequencies are then used to determine the thermal contribution to the Helmholtz free energy within the quasiharmonic approximation and derive the equation of state, heat capacity, and entropy.

I. INTRODUCTION

$MgSiO_3$ perovskite has long been a subject of numerous theoretical and experimental studies since it is generally thought to be the primary constituent of Earth's lower mantle. There has been considerable interest in the vibrational spectroscopy of perovskite as the lattice vibrations control its thermodynamical properties such as thermal expansion, specific heat and entropy. It is also interesting to understand the vibrational spectrum of a low symmetry structure like orthorhombic perovskite in which the phonon dispersions are discontinuous at the Brillouin-zone center.

Over last few years, nearly all optically active zone-center (Γ) modes of $MgSiO_3$ perovskite have been experimentally determined at ambient conditions.[1–3] Some Raman-active modes have been measured to pressure as high as 65 GPa at room temperature,[4,5] whereas some infrared modes have been measured up to 25 GPa.[1,6] Temperature dependence of Raman spectra has also been investigated at ambient pressure[2,7] and, more recently, at high pressure.[8] The lattice dynamical properties of perovskite (in stable orthorhombic and hypothetical cubic phases) have been studied theoretically using semiempirical and nonempirical model calculations.[4,9,10] Although first-principles studies of the structural and elastic properties of perovskites have been performed at high pressures,[11,12] its lattice-dynamical studies are limited to zero pressure and zone-center modes.[13] Here we apply a first-principles approach based on density-functional perturbation theory (DFPT), to determine the pressure dependence of phonon dispersion for $MgSiO_3$ perovskite to 150 GPa and to derive several thermodynamic quantities of interest, as in our recent study of MgO.[14]

II. METHOD

Computations are performed using density-functional perturbation theory[15] within the local-density approximation.[16] Pseudopotentials are generated for Mg by the method of von Barth and Car[17] whereas those for O and Si by the method of Troullier and Martins.[18] Plane-wave cutoff is set at 70 Ry and the Brillouin zone (Bz) is sampled using two special $\mathbf{k}$ points. The effects of using the larger cutoff of 80 Ry and four $\mathbf{k}$ points on the calculated properties are found to be insignificant.

The central quantity in the lattice-dynamical calculation is the dynamical matrix

$$\boldsymbol{D}^{\alpha\beta}_{\kappa\kappa'}(\mathbf{q}) = \frac{1}{\sqrt{m_\kappa m_{\kappa'}}} \sum_l \boldsymbol{\Phi}^{\alpha\beta}_{\kappa\kappa'}(0l)\exp[-i\mathbf{q}\cdot(\mathbf{x}_0-\mathbf{x}_l)]. \tag{1}$$

Here the interatomic force constants $\boldsymbol{\Phi}^{\alpha\beta}_{\kappa\kappa'}(0l)$ include ionic and electronic contributions, the former being calculated from Ewald sums and the latter being expressed as

$$\boldsymbol{\Phi}^{\alpha\beta}_{\kappa\kappa'}(0l)_{el} = \int \left[\frac{\partial\rho(\mathbf{r})}{\partial u^\alpha_\kappa(0)} \frac{\partial V_{ion}(\mathbf{r})}{\partial u^\beta_{\kappa'}(l)} + \rho(\mathbf{r}) \frac{\partial^2 V_{ion}(\mathbf{r})}{\partial u^\alpha_\kappa(0)\partial u^\beta_{\kappa'}(l)} \right] d^3r, \tag{2}$$

where $\rho(\mathbf{r})$ is the electron density, $V_{ion}(\mathbf{r})$ is the ionic potential, and $\partial\rho(\mathbf{r})/\partial u^\alpha_\kappa(0)$ represents the density response of the system to a displacement of the κ atom in the reference cell ($l=0$) along the α direction. This linear electron-density response can be calculated self-consistently using DFPT. It is convenient to treat lattice displacements with a given periodicity $\mathbf{q}$, $u^\alpha_\kappa(l) = \tilde{u}^\alpha_\kappa(\mathbf{q})\exp[i\mathbf{q}\cdot\mathbf{x}_l]$, since the corresponding linear density response has the same periodicity and the dynamical matrix, $D^{\alpha\beta}_{\kappa\kappa'}(\mathbf{q})$, and the corresponding phonons can be determined directly at any wave vector $\mathbf{q}$ in the BZ without the need for supercells. At a given pressure (or volume), first the orthorhombic structure is fully optimized.

TABLE I. Calculated frequencies (in cm^{-1}) and mode Grüneisen parameters of Raman modes compared with experiments at zero pressure. See text for comments on experimental mode assignment

	Calc.		Expt.	
Symmetry	ν_i	γ_i	ν_i	γ_i
A_g	234	2.66	249 [a], 245 [b]	2.14[b], 3.0 [c]
B_{2g}	258	2.39	254 [a], 251 [b]	2.06 [a]
B_{3g}	277	2.15		
A_g	281	1.54	282 [a], 279 [b]	1.39 [b], 1.6 [c]
B_{1g}	286	1.23		
B_{1g}	331	1.80	338 [a], 327 [b]	1.41 [b]
B_{3g}	338	1.15	343 [a], 334 [b]	1.63 [b]
B_{1g}	376	1.81	369 [a], 370 [b]	1.06 [b], 1.7 [c]
A_g	380	1.50	381 [a], 379 [b]	1.21 [b], 1.9 [c]
A_g	400	1.54	392 [a], 387 [b]	1.34 [b]
B_{2g}	438	1.21		
B_{3g}	445	2.00		
B_{1g}	512	1.26		
B_{2g}	518	2.46		
A_g	518	2.06	501 [a], 499 [b]	1.8 [b], 3.5 [c]
B_{3g}	541	2.33		
A_g	549	1.86	542 [a]	1.6 [c]
B_{1g}	616	1.29		
B_{2g}	623	1.21		
A_g	658	1.29	666 [a]	
B_{1g}	660	1.28		
B_{3g}	783	1.35		
B_{1g}	827	1.25		
B_{2g}	848	1.32	~900 [c]	0.7 [c]

[a]Reference 2.
[b]Reference 5.
[c]Reference 4.

Then the dynamical matrices are computed on $2\times2\times2$ **q** grid and are used for interpolation to obtain bulk phonon dispersions.

III. RESULTS AND DISCUSSION

A. Vibrational properties

The orthorhombic $MgSiO_3$ perovskite consists of a corner-linked network of SiO_6 octahedra, with Mg atoms surrounded by cages of eight octahedra. The unit cell consists of four formulas so there are 60 vibrations at any point in the Brillouin zone. At the zone center (Γ), three acoustic modes with symmetry

$$\Gamma_{ac}=B_{1u}+B_{2u}+B_{3u} \tag{3}$$

have zero frequencies. The irreducible representations of the optic modes are

$$\Gamma_{op}=7A_g(R)+7B_{1g}(R)+5B_{2g}(R)+5B_{3g}(R)+8A_u +7B_{1u}(IR)+9B_{2u}(IR)+9B_{3u}(IR). \tag{4}$$

Here, subscripts g and u represent symmetric and antisymmetric modes with respect to center of inversion. There are

TABLE II. Calculated frequencies (in $cm-1$) and mode Grüneisen parameters of infrared modes, compared with experiments at zero pressure. See text for comments on experimental mode assignment.

	Calc.			Expt. [a]		
Symmetry	ν_i(TO)	ν_i(LO)	γ_i	ν_i(TO)	ν_i(LO)	γ_i
B_{1u}	182	241	3.05	180	238	
				222	194	1.40 [c]
B_{2u}	251	260	1.92	247	252	1.76 [c]
B_{3u}	272	272	1.81	262	263	
B_{1u}	309	331	1.64	286	286	1.29 [c]
B_{3u}	326	361	1.90	317	364	1.49 [c]
B_{2u}	348	358	1.98	344	332	1.17 [c]
B_{2u}	391	396	2.06	388	389	1.28 [c]
B_{2u}	422	436	1.22		415	
B_{3u}	435	442	1.08	430	452	
B_{1u}	446	479	1.97	444	440	
B_{3u}	475	479	1.87	484	477	
B_{1u}	486	568	1.72	466	578	
B_{2u}	504	545	1.81	496	496	
B_{3u}	511	570	1.67	522 [b]		
B_{2u}	549	648	1.72	534,544 [b]	534	1.19 [b]
B_{3u}	574	574	1.54			
B_{3u}	597	710	1.38	597	727	
B_{1u}	598	684	1.37	614, 614 [b]	614	1.06 [b]
B_{2u}	675	718	1.39	679, 683 [b]	672	0.97 [b]
B_{1u}	710	712	1.80			
B_{3u}	711	739	0.93	705	702	
B_{1u}	723	914	1.67	721	721	
B_{2u}	761	774	0.98			
B_{2u}	776	952	1.26	771	943	
B_{3u}	781	943	1.52	780, 797 [b] 877	780	0.99 [b]

[a]Reference 3.
[b]Reference 1.
[c]Reference 6.

24 Raman-active (R), 25 infrared-active (IR) modes, and 8 A_u optically silent modes. The calculated eigenvectors are used to deduce the symmetry labels of the modes. Inspection of the eigenvectors allows us to visualize the vibrations in terms of internal and external motions of the SiO_6 octahedra and motion of Mg ions. The predicted zone-center phonon frequencies are given in Tables I, II, III.

Symmetry assignments are, however, difficult in the experiments. Therefore, precise comparisons between the theory and experiment are not possible, but we find a close correspondence in frequency. Our results show that Raman modes range from 234 to 848 cm^{-1} in frequency. The observed data of ~249 to 666 cm^{-1} of intense Raman bands[2] can be associated with the calculated range of 234 to

TABLE III. Calculated frequencies (in $cm-1$) and mode Grüneisen parameters of A_u inactive modes at zero pressure.

ν_i	182	277	365	384	497	610	662	751
γ_i	0.86	1.94	1.20	0.99	2.02	1.25	2.12	1.67

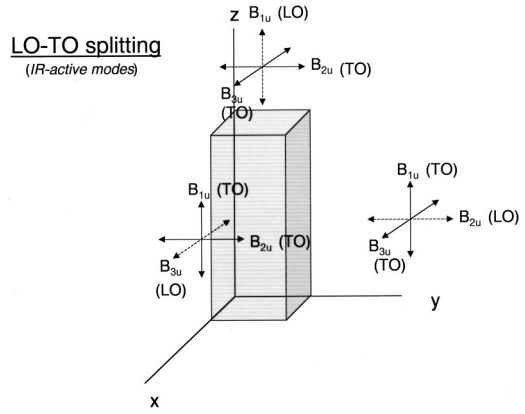

FIG. 1. Sketch describing the LO and TO infrared-active modes.

658 cm^{-1} for A_g modes (Table I). Raman modes do not involve displacements of Si ions as they occupy the centrosymmetric positions. The lowest frequency A_g(234 cm^{-1}) and B_{3g}(277 cm^{-1}) modes can be viewed as mostly SiO_6 octahedral rocking motion whereas the lowest frequency B_{1g}(286 cm^{-1}) and B_{2g}(258 cm^{-1}) modes are mainly associated with Mg motion. The octahedral de-

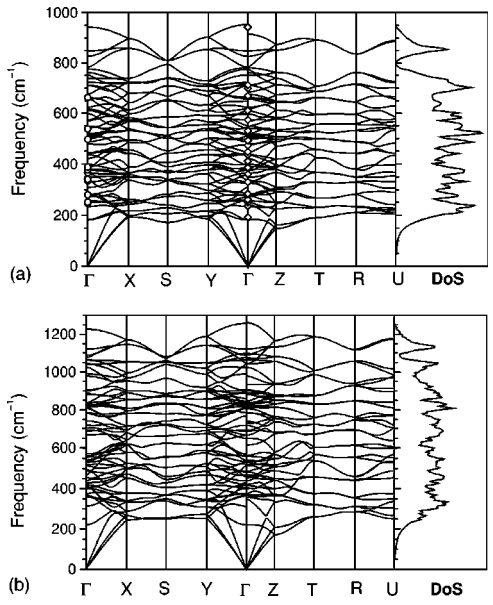

FIG. 2. Phonon dispersion and density of states for $MgSiO_3$-perovskite (a) 0 and (b) 100 GPa. Experimental data are from (Refs. 1–3, 5, and 6).

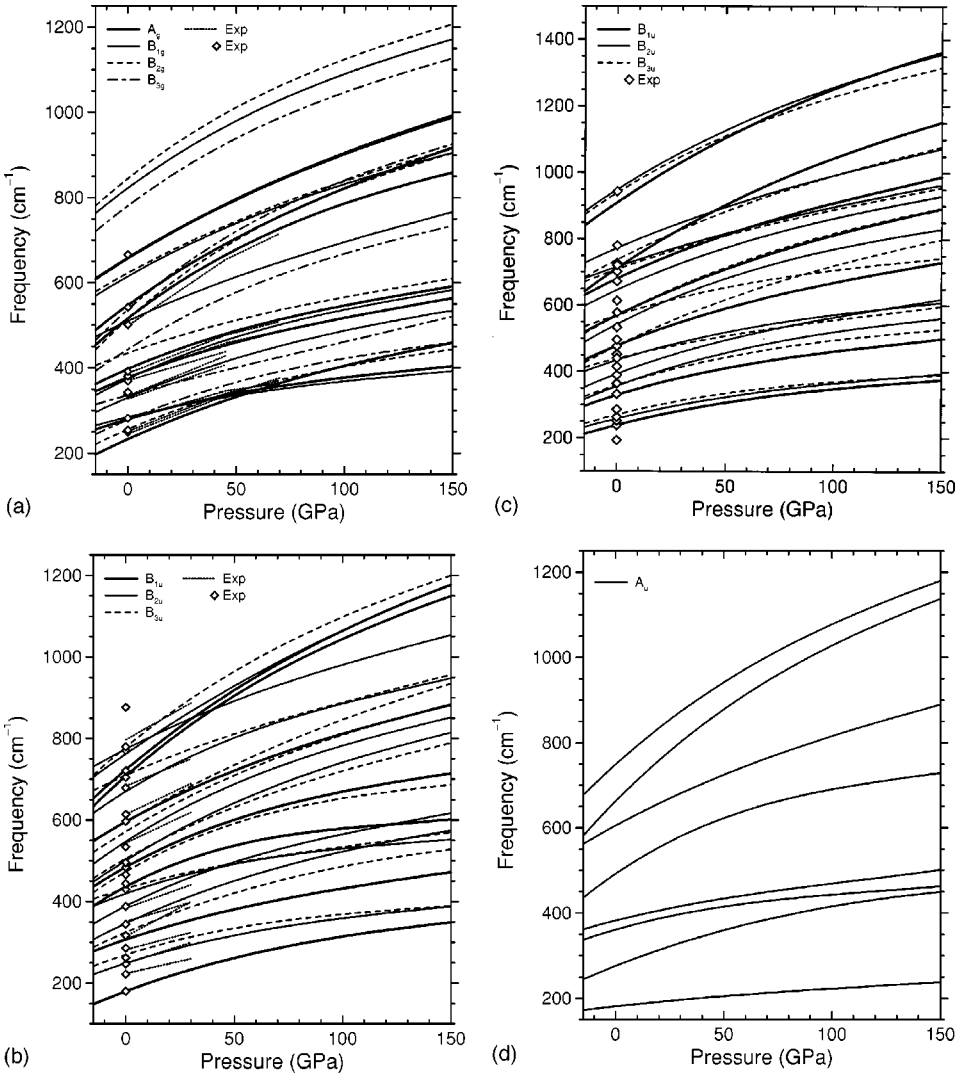

FIG. 3. Pressure dependence of the frequencies of (a) Raman, (b) Infrared TO, (c) Infrared LO (d), and silent modes at the zone center. Experimental data are from (Refs. 1–3, 5, and 6).

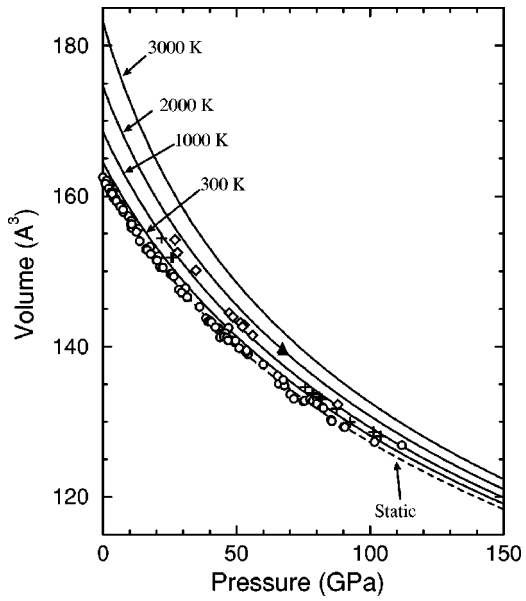

FIG. 4. Pressure-volume equations of state for the static lattice and along 300, 1000, 2000, and 3000 K isotherms. Experimental data at corresponding temperatures are denoted by circles, crosses, diamonds, and triangles (Refs. 19–21, 23, and 22).

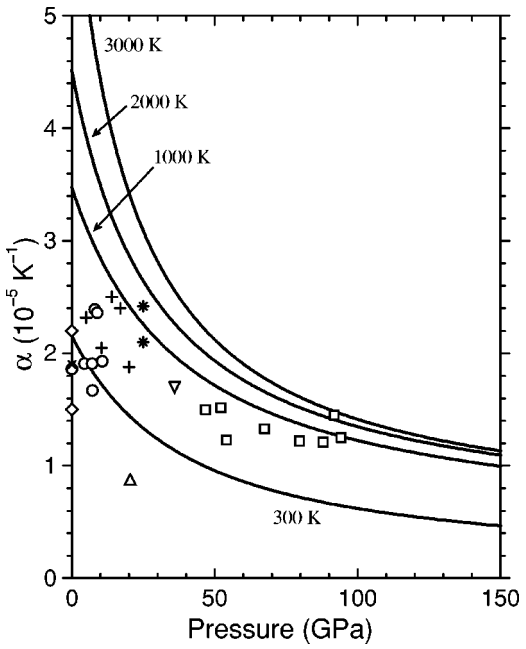

FIG. 5. Coefficient of thermal expansion along 300, 1000, 2000, and 3000 K isotherms. Symbols are the experimental data for $\alpha_{\langle T_1-T_2\rangle}$ averaged between temperatures T_1 and T_2. Diamonds (Ref. 25) are $\alpha_{\langle 77-298\rangle}$ and $\alpha_{\langle 298-383\rangle}$; cross (Ref. 26) is $\alpha_{\langle 150-373\rangle}$; and circles (Ref. 24) are $\alpha_{\langle 295-404\rangle}$, $\alpha_{\langle 300-1076\rangle}$, $\alpha_{\langle 306-880\rangle}$, $\alpha_{\langle 625-1174\rangle}$, $\alpha_{\langle 207-1276\rangle}$, $\alpha_{\langle 625-1074\rangle}$, and $\alpha_{\langle 677-1024\rangle}$ with increasing pressure; pluses (Ref. 29) are $\alpha_{\langle 300-1200\rangle}$ at 20 GPa and $\alpha_{\langle 300-800\rangle}$ at lower pressures; up triangle (Ref. 28) is α_{300}; down triangle (Ref. 27) is α_{300}; stars (Ref. 21) are α_{1000} and α_{2000}; finally squares (Ref. 22) are $\alpha_{\langle 300-1918\rangle}$, $\alpha_{\langle 300-1889\rangle}$, $\alpha_{\langle 300-2372\rangle}$, $\alpha_{\langle 300-2897\rangle}$, $\alpha_{\langle 300-1681\rangle}$, $\alpha_{\langle 300-1995\rangle}$, $\alpha_{\langle 300-1380\rangle}$, and $\alpha_{\langle 300-1179\rangle}$ with increasing pressure.

formation increasingly dominates at higher frequencies. The highest frequency $A_g(658\ \mathrm{cm}^{-1})$, $B_{1g}(827\ \mathrm{cm}^{-1})$, $B_{2g}(848\ \mathrm{cm}^{-1})$, and $B_{3g}(783\ \mathrm{cm}^{-1})$ are nearly pure octahedral deformational modes involving tilting or stretching of the SiO_6 octahedra.

The predicted frequencies of the *IR* modes at Γ range from 182 to 952 cm^{-1}, in agreement with lower ($\sim$180 cm^{-1}) and upper ($\sim$950 cm^{-1}) limits set by measurements of the LO and TO frequencies of 23 IR modes.[3] All the measured TO frequencies except two (222 and 870 cm^{-1}) can be reconciled with the calculated values; our result for the highest TO frequency is 781 cm^{-1}, compared to the reported value of 870 cm^{-1} (Table II). Unlike *R* modes, all *IR* modes involve significant octahedral deformations such as asymmetric stretching and bending of SiO_6 octahedra although lower frequency modes also involve large Mg motion.

The frequency of an infrared active mode splits into two values according to whether the mode is longitudinal (LO) or transverse (TO). This is due to the contribution of the macroscopic electric field to the LO mode in a polar crystal. There are 25 of these modes and 50 different frequencies at zone center (Table II). These correspond to various B_{1u}, B_{2u}, and B_{3u} modes, which are related through cyclic permutations of *x*, *y*, and *z*, the Cartesian coordinates, in real space (Fig. 1). The B_{1u}, B_{2u}, and B_{3u} modes are LO (TO) when $\mathbf{q}$ approaches Γ along the q_z (q_x or q_y), q_y (q_z or q_x), and q_x (q_y or q_z) directions, respectively, thus the phonon-dispersion curves showing discontinuities at Γ (Fig. 2). Such behavior at the zone center is characteristic of a low symmetry structure such as orthorhombic perovskite.

The nonanalytical contribution of the macroscopic electric field to the force-constant tensor is given by

TABLE IV. Calculated equation of state parameters at zero pressure compared with experiments (Ref. 19, 20, 24, and 25)

	300 K Calc.	300 K Expt.	1000 K Calc.	2000 K Calc.
V(Å^3)	164.1	162.5	167.6	174.4
K_T(GPa)	247	246–272	222	181
$\partial K_T/\partial P$	3.97	3.9–4.0	4.19	4.67
$\partial^2 K_T/\partial P^2$ (GPa^{-1})	−0.016		−0.030	−0.062
$\partial K_T/\partial T$ (GPa K^{-1})	−0.031	−0.023 to −0.072	−0.038	−0.044
$\alpha(\times 10^{-5}\mathrm{K}^{-1})$	2.15	1.7–2.2	3.48	4.52

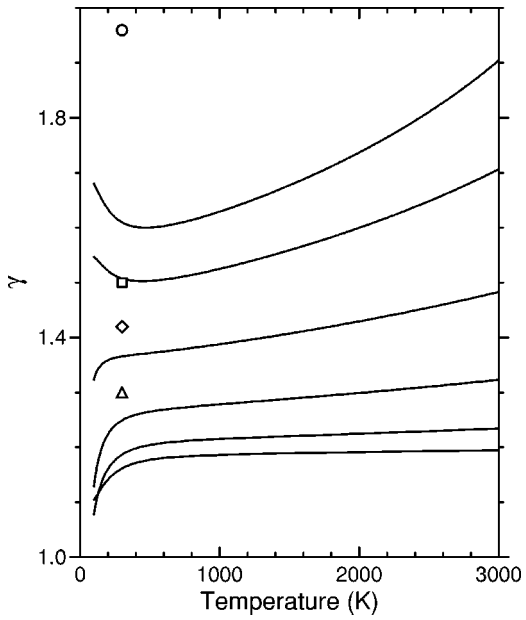

FIG. 6. Temperature dependence of thermal Grüneisen parameter along the isobars at 0, 10, 30, 60, 100, and 150 GPa (solid lines from top to bottom). Previous results derived from experiments are denoted by symbols (Refs. 5, 7, 20, and 30).

$$\frac{4\pi e^2}{V}\frac{(\mathbf{q}\cdot\mathbf{Z}^*_\kappa)_\alpha(\mathbf{q}\cdot\mathbf{Z}^*_{\kappa'})_\beta}{\mathbf{q}\cdot\boldsymbol{\epsilon}_\infty\cdot\mathbf{q}}, \tag{5}$$

where the tensors $\mathbf{Z}$ and $\boldsymbol{\epsilon}_\infty$ are, respectively, the Born effective charges and macroscopic high-frequency static dielectric constant which are calculated self-consistently. The diagonal components of the dielectric tensor are 3.33, 3.34, and 3.32 at zero pressure, and they are shown to decrease slightly with increasing pressure (3.11, 3.13, and 3.17 at 100 GPa). The Born effective charges for Mg and Si are close to the formal ionic charges of magnitudes equal to 2 and 4, and are weakly anisotropic: $Z^*(\mathrm{Mg})=(2.07,2.07,2.16)$ and $Z^*(\mathrm{Si})=(3.92,3.93,3.94)$ at zero pressure, and $Z^*(\mathrm{Mg})=(1.95,1.89,2.06)$ and $Z^*(\mathrm{Si})=(3.73,3.78,3.76)$ at 100 GPa. However, those for O(1) and O(2) are significantly different from the ideal value of 2 and are highly anisotropic: $Z^*[\mathrm{O}(1)]=(-1.72,-1.61,-2.76)$ and $Z^*[\mathrm{O}(2)]=(-2.21,-2.30,-1.72)$ at zero pressure, and $Z^*[\mathrm{O}(1)]=(-1.71,-1.58,-2.54)$ and $Z^*[\mathrm{O}(2)]=(-2.05,-2.14,-1.74)$ at 100 GPa.

The splitting of the softest B_{1u} (182 cm^{-1}) mode is 59 cm^{-1}, compared to the observed value of 58 cm^{-1},[3] however, the softest B_{2u} and B_{3u} modes do not show any significant splitting (Table II). The three hardest B_{1u}, B_{2u}, and B_{3u} modes (at 723, 776, and 781 cm^{-1}), respectively, show the largest splittings of 191, 176, and 162 cm^{-1}, respectively. This is comparable to the observed value of 172 cm^{-1} of an *IR* mode at 771 cm^{-1}.[3] The large splittings are also shown by the modes near 500 and 600 cm^{-1}. The calculated LO frequency is always greater than the corresponding TO frequency as expected since the macroscopic electric field stiffens the force constants. Experimental data show this trend clearly for intense bands but an opposite trend for several other modes.[3]

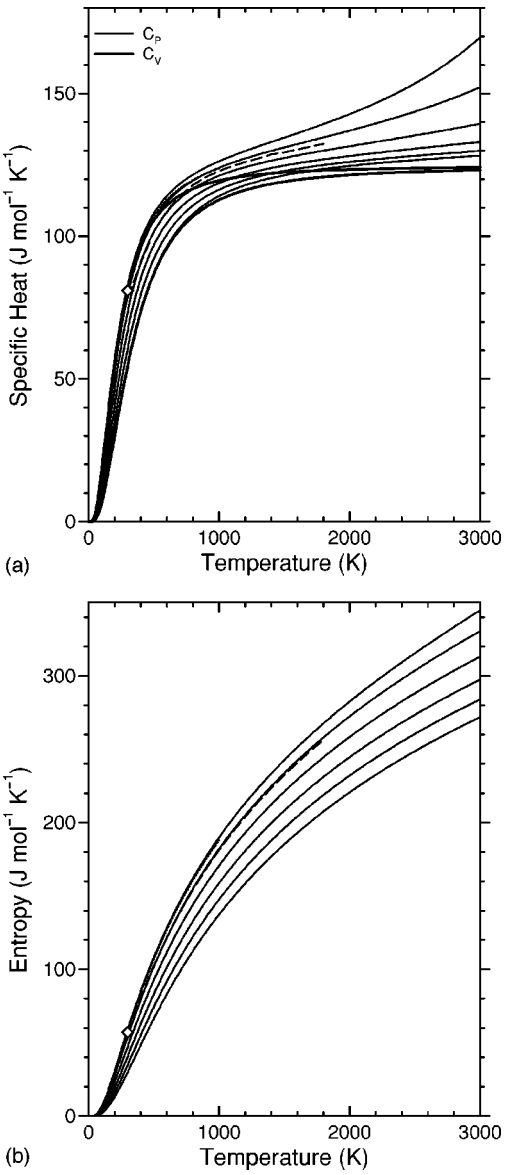

FIG. 7. Temperature dependence of (a) heat capacity and (b) entropy along the isobars at 0, 10, 30, 60, 100, and 150 GPa (solid lines from top to bottom). Previous results derived from experiments are denoted by dotted line (Ref. 5) and by dashed line (Ref. 31). Direct experimental value at ambient condition (Ref. 32) is denoted by symbol.

All mode frequencies are shown to be positive and also to increase with increasing pressure indicating the dynamical stability of an orthorhombic perovskite (Figs. 2 and 3). The calculated pressure derivatives ($d\omega_i/dP$) and mode Grüneisen parameters ($\gamma_i=-d\ln\omega_i/d\ln V$) span the ranges of 0.6–4.8 $\mathrm{cm}^{-1}\mathrm{GPa}^{-1}$, and 0.3–3.1, respectively, at zero pressure. These compare favorably with observed ranges of 1.2 to 4.2 $\mathrm{cm}^{-1}\mathrm{GPa}^{-1}$, and $\sim$1 to 3.5 for 20 mode frequencies, and theory reproduces the experimental pressure dependences very well (Fig. 3).[1,4–6] In contrast, the potential-induced breathing model[4] predicted γ_i's as high as 6.8. Two of the acoustic branches show the smallest values ($\sim$0.3) in the Γ-Z direction near Γ whereas the lowest frequency A_g and B_{1u} modes show the largest values of γ_i. All γ_i's are shown to decrease with increasing pressure; their values vary from 0.2 to 1.91 at 100 GPa. No abrupt changes in pressure-

frequency shifts of Raman modes around 40 GPa as shown by spectroscopic data are predicted.[5]

Present results agree with experiments better than earlier predictions do. Our calculated overall variation in the frequency at Γ is 182–952 cm^{-1}, consistent with the variation of ~180–950 cm^{-1} reported by experiments.[2,3] The corresponding results are ~130–1300 cm^{-1} from modified electron gas model,[9] 95–1363 cm^{-1} from the potential-induced breathing model,[4] and ~170–850 cm^{-1} from semiempirical molecular dynamics.[10] The previous pseudopotential result of ~150–864 cm^{-1} corresponds only to TO modes.[13]

B. Thermodynamical properties

When the volume dependence of the thermal energy is represented within the quasiharmonic approximation (QHA), the Helmholtz free energy takes the following form:

$$F(V,T)=U_0(V)+\frac{1}{2}\sum_{\mathbf{q},j} h\omega_j(\mathbf{q},V) + k_BT\sum_{\mathbf{q},j} \ln[1-\exp(-h\omega_j(\mathbf{q},V)/k_BT)], \quad (6)$$

where the first, second, and third terms are, respectively, the internal, zero-point, and thermal contributions. The summation includes 1728 points in the Brillouin zone to get the full convergence. The QHA is expected to work well over a wide temperature range at elevated pressures although it tends to overestimate the thermal effects at high temperatures and zero pressure. This has been justified by extensive and successful comparisons between theory and experiments in our recent study of MgO.[14]

A series of the calculated equation of state (EoS) isotherms obtained by fitting the fourth-order finite strain equation to the calculated free energy versus volume result at each temperature are shown in Fig. 4. Our results are slightly shifted upwards relative to the experimental data.[19–23]. The corrections for the zero-point motion and room temperature are a 2% increase in volume and a 5% decrease in bulk modulus from their athermal values given by the static calculations. Our theoretical results for the equation-of-state parameters of perovskites at ambient conditions fall within the ranges of the experimental variation (Table IV).

The coefficient of thermal expansion $\alpha=(1/V)(\partial V/\partial T)_P$ is determined from the temperature variation of volume at each pressure (Fig. 5). At zero pressure, the predicted temperature dependence of α appears to be significantly biased by the QHA leading to unusually large values at very high temperatures. As pressure rises, α rapidly decreases at each temperature, and also the effects of temperature are increasingly suppressed, thus converging to a nearly constant value in the limit of high pressure and high temperature. Our results are consistent with the experimental data within the existing large uncertainties.[21,22,24–29]

The thermal Grüneisen parameter is defined as $\gamma=\alpha VK_T/C_V$, where C_V is the heat capacity at constant volume. The predicted value of γ is 1.61 at ambient condition, compared to the relatively wide variation of 1.3–1.96 reported previously.[5,7,30,31] As pressure rises, γ rapidly decreases with the temperature-induced variations in it strongly suppressed at high pressures (Fig. 6). Accordingly, the value of $q=(\partial \ln \gamma/\partial \ln V)_T$ decreases from ~2 to 0.1 from 0 to 150 GPa, remaining nearly independent of temperature.

The specific heat at constant pressure (C_P) calculated by using $C_P=C_V(1+\alpha\gamma T)$ and the entropy (S) are shown in Fig. 7. The ambient value for C_V is 81.85 $J\,mol^{-1}\,K^{-1}$ and for C_P is 82.70 $J\,mol^{-1}\,K^{-1}$ in an excellent agreement with the value of $C_P=78$ $J\,mol^{-1}\,K^{-1}$ from the calorimetric measurements.[32] Similarly the calculated value of 58.72 $J\,mol^{-1}\,K^{-1}$ for S compares favorably with the measured value of 57.2 $J\,mol^{-1}\,K^{-1}$.[32] The calculated C_P and S at high T (zero pressure) compare well with the previously reported values (Fig. 7).

IV. SUMMARY

We have reported *ab initio* phonon dispersion and density of states for $MgSiO_3$-perovskite, the main Earth-forming mineral phase, throughout the relevant pressure range in the planet's interior. These were obtained using density-functional perturbation theory. Experimentally only some of the phonon frequencies are known at the Brillouin-zone center in a much more limited pressure range. Thermodynamical properties were then derived using the quasiharmonic approximation. All these quantities, which are fundamental to understanding geophysical processes, are only approximately known, usually by uncertain extrapolations, in the P-T range reported here. Therefore, our predictive results represent a significant step towards the understanding of this mineral.

ACKNOWLEDGMENTS

This work was supported by NSF Grant No. EAR-9973130. Computing facilities were provided by the Supercomputing Institute for Digital Technology (SIDT). B.B.K. acknowledges financial support from SIDT. S.d.G. and S.B. acknowledge support from MURST under the initiative *Progetti di ricerca di rilevante interesse nazionale*.

[1] Q. Williams, R. Jeanloz, and P. McMillan, J. Geophys. Res. **92**, 8116 (1987).
[2] D.J. Durben and G.H. Wolf, Am. Mineral. **77**, 890 (1992).
[3] R. Lu, A.M. Hofmeister, and Y. Wang, J. Geophys. Res. **99**, 11 795 (1994).
[4] R.J. Hemley, M.D. Jackson, and R.G. Gordon, Phys. Chem. Miner. **14**, 2 (1987).
[5] A. Chopelas, Phys. Earth Planet. Inter. **98**, 3 (1996).
[6] R. Lu and A.M. Hofmeister, Phys. Chem. Miner. **21**, 78 (1994).
[7] P. Gillet, F. Guyot, and Y. Wang, Geophys. Res. Lett. **23**, 3043 (1996).
[8] P. Gillet, I. Daniel, F. Guyot, J. Matas, and J.C. Chervin, Phys. Earth Planet. Inter. **117**, 361 (2000).
[9] G.H. Wolf and M.S.T. Bukowinski, in *High Pressure Research Mineral Physics*, edited by M.H. Manghani and Y. Syona (American Geophysical Union, Washington, DC, 1987), p. 313.

[10] B. Winker and M.T. Dove, Phys. Chem. Miner. **18**, 407 (1992).
[11] R.M. Wentzcovitch, J.L. Martins, and G.D. Price, Phys. Rev. Lett. **70**, 3947 (1993).
[12] B.B. Karki, L. Stixrude, S.J. Clark, M.C. Warren, G.J. Ackland, and J. Crain, Am. Mineral. **82**, 635 (1997).
[13] M.C. Warren and G.J. Ackland, Phys. Chem. Miner. **23**, 107 (1996).
[14] B.B. Karki, R.M. Wentzcovitch, S. de Gironcoli, and S. Baroni, Science **286**, 1705 (1999); Phys. Rev. B, **58**, 8793 (2000).
[15] S. Baroni, P. Giannozzi, and A. Testa, Phys. Rev. Lett. **58**, 1861 (1987); P. Giannozzi, S. de Gironcoli, P. Pavone, and S. Baroni, Phys. Rev. B **43**, 7231 (1991).
[16] J.P. Perdew and A. Zunger, Phys. Rev. B **23**, 5048 (1981).
[17] U. von Barth and R. Car (unpublished).
[18] N. Troullier and J.L. Martins, Phys. Rev. B **43**, 1993 (1991).
[19] E. Knittle, R. Jeanloz, and G.L. Smith, Nature (London) **319**, 214 (1986).
[20] H.K. Mao, R.J. Hemely, Y. Fei, J.F. Shu, L.C. Chen, A.P. Jephcoat, Y. Wu, and W.A. Basset, J. Geophys. Res. **96**, 8069 (1991).
[21] N. Funamori, T. Yagi, W. Utsumi, T. Kondo, and T. Uchida, J. Geophys. Res. **101**, 8257 (1996).
[22] G. Fiquet, A. Dewaele, D. Andrault, M. Kunz, and T.L. Bihan, Geophys. Res. Lett. **27**, 21 (2000).
[23] S. Saxena, L.S. Dubrovinsky, T. Faramarz, and T.L. Bihan, Am. Mineral. **84**, 226 (1999).
[24] Y. Wang., D.J. Weidner, R.C. Liebermann, and Y. Zhao, Phys. Earth Planet. Inter. **83**, 40 (1994).
[25] N.L. Ross and R.M. Hazen, Phys. Chem. Miner. **17**, 228 (1989).
[26] J.B. Parise, Y. Wang, Yeganeh-Haeri, D.E. Cox, and Y. Fei, Geophys. Res. Lett. **17**, 2089 (1990).
[27] N. Funamori and T. Yagi, Geophys. Res. Lett. **20**, 387 (1993).
[28] H. Morishima, E. Ohtani, T. Kato, O. Shimomura, and T. Kikegawa, Geophys. Res. Lett. **21**, 899 (1994).
[29] W. Utsumi, N. Funamori, T. Yagi, E. Ito, T. Kikegawa, and O. Shimomura, Geophys. Res. Lett. **22**, 1005 (1995).
[30] L. Stixrude, R.J. Hemley, Y. Fei, and H.K. Mao, Science **257**, 1099 (1992).
[31] O.L. Anderson, K. Masuda, and D.G. Isaak, Phys. Earth Planet. Inter. **98**, 31 (1996).
[32] M. Akaogi and E. Ito, Geophys. Res. Lett. **20**, 105 (1993).